Wideband Antennas for Cubesat Platforms: Design and Multiphysics Analysis

Matteo B. Lodi, Giacomo Muntoni
Department of Electrical and Electronic Engineering
University of Cagliari
via Marengo 3, Cagliari 09123, Italy
{matteob.lodi; giacomo.muntoni}@unica.it

Marco Simone
Department of Electrical, Electronics, and Computer Engineering (DIEEI)
University of Catania
Catania 95125, Italy
marco.simone@unict.it

Alessandro Fanti, Giuseppe Mazzarella
Department of Electrical and Electronic Engineering
University of Cagliari
via Marengo 3, Cagliari 09123, Italy
{alessandro.fanti; mazzarella}@unica.it

***Abstract*—The paradigm of new space economy is demanding for innovative, cost-effective solutions to enable future missions. To this aim, CubeSat platforms proved to play a key role. The communication sub-system is crucial for these nanosatellites, and the antenna is the core element. To push the forefront, the challenging field of CubeSat antennas design demands for innovative design methodologies, new materials and disruptive manufacturing approaches, such as additive manufacturing. Considering specific mission requirements, combined with the harsh space environment, a given antenna layout must effectively perform. To this aim, multiphysics simulations can help in discriminating between different design, while favoring the understanding of potential risky situations. This work deals with the presentation of methodologies for designing innovative antennas for CubeSat applications. In particular, a 3D-printed curved stacked patch antenna working in the S-band and a stacked patch antenna array working in the Ka-band will be presented. The electromagnetic performances of the antennas have been studied with a numerical multiphysics model considering the thermal and mechanical variations during a simulated CubeSat mission.**

Keywords—Cubesat antennas, wideband antennas, 3-D printing, S-band, Ka-band

I. INTRODUCTION

Today, the space industry and economy are facing a revolution, sustained by the new paradigm of considerable private investments focused on a prompt revenue. Given the aim of enabling future missions, the challenge of providing cost-effective solutions, to be developed in short time, is urgent. In this framework, a class of miniaturized satellites, called CubeSats, represents an appealing opportunity for Earth observation, scientific missions, communication and/or surveillance purposes. CubeSats are nanosatellites having size of 10 cm × 10 cm × 10 cm (1U) and a mass of 1.3 kg. They are a versatile platform and are increasingly employed for missions in the Low Earth Orbit (LEO). Indeed, from of 1st January 2021, more than 1,357 CubeSats have been launched [1]. A rather crucial aspect of a CubeSat and a key factor for the success of its mission is the communication module, whose core element is the antenna. So far, there is not a shared approach for designing CubeSat antennas, outside of the mechanical and electrical constraints demanded by the specifications [1]. It is therefore mandatory to explore innovative approaches for designing this sub-system.

CubeSat can have different communication systems working in different frequency bands. In particular, the S-band, i.e., from 2.0 to 2.2 GHz (uplink: 2.025-2.11 GHz, downlink: 2.2-2.29 GHz), has been used for telemetry, tracking and command (TT&C) applications [2], [3]. Also, the X-band (7.9-8.4 GHz) has been considered for CubeSat missions, especially for deep space network (DSN) applications [3]. Recently, the Ka-band ($26 - 34.7$ GHz for down- and uplink) has been explored. To the stringent communications requirements (e.g., gain, bandwidth, polarization, etc.), the possibility of adopting a given antenna design for a CubeSat mission depends on the material, the size, the weight, and other nontrivial aspects. Given these peculiar needs arising from the hostile space environment, several research efforts have been spent on the investigation of the antenna designs that are suitable for fly and be implemented on CubeSats. Therefore, there is a prolific CubeSat antenna literature [3]. So far, few K/Ka-band antenna designs have been proposed for CubeSat deep space missions. For instance, recently, a wideband microstrip patch antenna for Ka-band ($27 - 40$ GHz) CubeSat applications has been proposed [4]. The antenna is a square patch antenna, printed on FR4 slab, that achieved a 20.2% ($25.5 - 31.2$ GHz) -10 dB impedance bandwidth, while presenting an efficiency of 82%, and a 6.9 dB measured peak realized gain at 28 GHz [4].

It is feasible to satisfy the communication performances requirements using standard materials and canonical manufacturing techniques. However, due to the harsh and hostile space environment, combined with a given mission needs, unconventional materials and new manufacturing approaches have been considered for CubeSat antenna design. Especially considering costs and payload wegiths as key aspects. For instance, additive manufacturing (AM) and 3-D printing have been explored. Indeed, recently, a Ka-band passive multi-beam lens antenna for CubeSat space communication has been proposed in [5]. A half-ellipsoid lens has been 3-D printed using stereolithography (STL). The antenna gain is about $14 - 16$ dBi [5]. On the other hand, by using AM and 3-D printing, a self-deployable circularly polarized (CP) stacked Yagi–Uda phased antenna array operating at C-band ($5.6 - 6.0$ GHz) has been investigated in [6]. The array has been integrated into the top side of a 1U CubeSat via 3-D printed self-deployable spring hinges and frame. The self-deployable phased antenna array achieved 13.5 dBi, while possessing left-handed circular polarized gain and $\pm 10°$ beam steering angle [6]. The possibility of adopting these versatile, cost-effective and innovative materials and manufacturing approaches, however, calls for specific investigations to unravel their potential for space applications and for CubeSat antennas.

In this work, we will present different methodologies for designing innovative antennas for CubeSat applications. In particular, a 3D-printed curved stacked patch antenna working

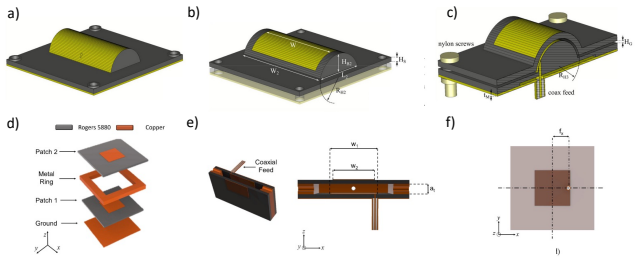

Fig. 1. Antenna Topologies: 3-D Printed Curved Patch Antenna: a) top layer. b) cut view. c) detail of the curvature radius. Ka-Band Stacked Patch Array: d) 3-D layout of the stacked patch antenna. e) side and cut view. f) feed position.

in the S-band and a stacked patch antenna array working in the Ka-band will be presented. Furthermore, the variation of the antennas performances have been studied with a numerical multiphysics model considering the thermal and mechanical conditions during a simulated CubeSat mission.

II. Antenna Topologies

A. 3-D Printed Curved Patch Antenna for S-Band

The possibility of designing a plastic, lightweight antenna to be manufactured using fused deposition modeling (FDM) 3-D printing has been investigated. A stacked antenna consisting of a bottom and a top layer has been considered (Fig. 1a-1c). The bottom layer layout is similar to a bended rectangular patch antenna [6]. In this work, the selected substrate material is Acrylonitrile Butadiene Styrene thermoplastic filament (ABS - Sunlu Company, $\varepsilon_r = 2.3$, $\tan\delta = 0.01$ at 2.15 GHz). The substrate has a volume of 71.5 mm x 71.5 mm x 2.5 mm. The substrate is topped by an ABS cylindrical protrusion having a bending radius $R_H = 12$ mm. The cylindrical protrusion footprint is long $W = 50.6$ mm along the x-direction and $L = 23.81$ mm along the y-direction, as shown in Fig. 1b. The metallization bent bottom aluminum patch (thickness $t_P = 50$ µm) is placed over the cylindrical protrusion. The height of the cylinder above the flat substrate is $H_B = R_H\,[1 - \cos(\arcsin L/(2R_H))] = 10.5$ mm. The bottom patch is fed by a commercial coaxial connector, placed at distance $y_f = 11.25$ mm from the center of the substrate (see Fig. 1b). A rectangular W x $L1 = 45$ mm x $H_A = 1$ mm air gap has been placed inside the bottom substrate, in direct contact with the ground plane. The ground plane is an aluminum plate ($\sigma = 3.5 \cdot 10^7$ Sm^{-1}, thickness $t_M = 0.9$ mm). Four holes (diameter $D_H = 5$ mm) are placed at the structure corners to allow sealing through nylon screws and nuts. Hollow pillars (diameter $D_P = 7.1$ mm) separates the holes while acting as spacers between the two layers (gap $H_G = 1$ mm). As shown in Fig. 1c, the top layer is 2.5 mm thick. The parasitic aluminum patch (thickness t_P) is set over a cylindrical surface with bending radius $R_{H2} = 15.5$ mm, and by a planar footprint equal to $W_2 = 60.6$ mm x $L_2 = 29.33$ mm. This second cylindrical shape has a height from the top flat substrate equal to $H_{B2} = 10.5$ mm. As a result, the overall height of the antenna is 17.4 mm. Hence, the lower profile curvature radius is $R_{H3} = R_H + H_G = 13$ mm.

The geometrical parameters have been simulated to obtain the best performance in terms of efficiency and to properly cover the S-band uplink and downlink frequency bands (uplink: $2.025 - 2.11$ GHz, downlink: $2.2 - 2.29$ GHz). CST Studio Suite (3DS, DE) has been used.

A prototype of the final antenna layout has been manufactured by using commercial 3D printer Raise 3D N2 Plus and characterized as explained in [7].

B. Stacked Patch Antenna Array for Ka-Band

The other case study, is a stacked patch antenna (Fig. 1d-1f) which has to cover both the downlink and uplink Ka-band, i.e., $31.8 - 32.3$ GHz and $34.2 - 34.7$ GHz, respectively. The proposed stacked patch antenna is based on two square Rogers RT/duroid 5880 dielectric slabs, 0.254 mm thick, which support two square metallic patches (w_1 and w_2 wide for bottom and upper patch, respectively. Rogers RT/duroid 5880 ($\epsilon_r = 2.2$, at 25°C, -125 ppm/°C, $CTE = 31 - 237$ ppm/°C) is a cheap substrate, and it has been tested and approved for space [8]. The Rogers layers are separated by an air gap (with thickness a_t), as shown in Fig. 1e. The upper substrate is sustained by a metal ring, in which small holes opened to allow the air outflow during the take-off step. Copper is the conductor material ($\sigma = 5.9 \cdot 10^7$ Sm^{-1}). The lower substrate is ground backed, whereas the upper substrate is sustained by a metallic ring. A coaxial cable is employed as feed (Fig. 1c-1f). The feed is placed at a distance f_x from the patch center. It must be reported that a little hole with a diameter $d = 0.30 < \lambda_0/30$ mm is considered. The hole allows the air to flow outside, as shown in Fig. 1e. The hole characteristic presence does not affect the electromagnetic performance of the antenna.

This geometry has been proposed and it has been optimized by using the following strategy [8]: the Particle Swarm Optimization (PSO) algorithm and CST Microwave Studio as full-wave electromagnetic analysis tool have been used in a synergistic way. In detail, the optimization process within the algorithm involved the size of the following antenna geometrical parameters, namely the bottom patch width w_1, the upper patch width w_2, the air gap thickness a_t, the feeding point position f_x, aiming to maximize the -10 dB frequency band in the interval $f \in (f_{min} = 30, f_{max} = 36)$ GHz. The optimization algorithm, developed in Matlab 2021b (The MathWorks Inc., MA USA) initializes the PSO parameters, inputting them in CST for evaluating the antennas performances through a full-wave simulation. Then, the script evaluates the fitness from the results from CST and iterates the swarm movement until the minimum of the objective function is reached [8]. A swarm of 10 particles is considered. Since the full-wave simulations are a relevant computational burden, the solution space position already encountered by the swarm are evaluated without re-simulating the antenna, thus reducing the computational load to less than 40%.

III. Multiphysics Analysis

The current state-of-the-art does not analyze if the thermal conditions experienced during the harsh LEO environment could affect the antenna operations and performances. An *in silico* thermo-mechanical analysis can help understand if a given antenna layout can be damaged or fail due to the mechanical stresses induced by the temperature gradients during the orbital cycles.

A. Thermal Modeling

In LEO environment, a CubeSat antenna is subject to different thermal loads. In this work, we consider as a case study a sun-synchronous circular orbit, with a right ascension

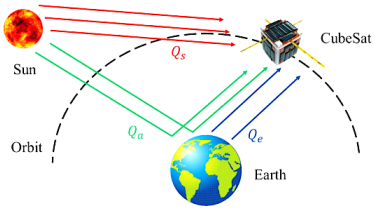

Fig. 2. Pictorial representation of the heat contributions and the thermal conditions faced by an antenna during a typical CubeSat mission.

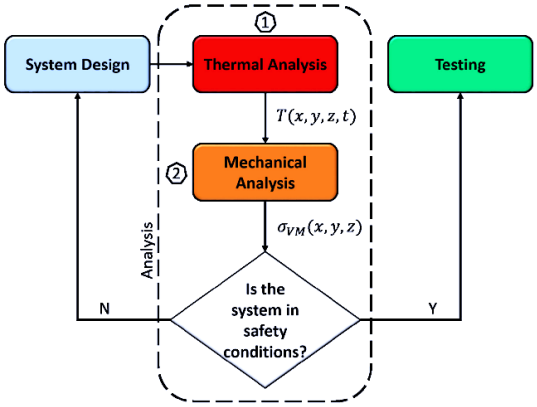

Fig. 3. Proposed numerical resolution scheme for the multiphysics model.

of ascending node of about 106°, orbital height of 300 km and an inclination of ~ 90°. We consider a total period of 3-5 orbits, with a 1 min time step. In these conditions, the direct solar radiation (Q_s, Wm^{-2}), the infrared energy emitted by Earth (Q_e), and Earth-reflected sunlight radiation, or albedo radiation (Q_a) are the heat sources that can vary the system temperature, as shown in Fig. 4. The spatio-temporal evolution of the temperature of the CubeSat and of the antenna is ruled by the following non-linear second order partial differential heat transfer balance equation [7], [8]

$$\rho C_p \frac{\partial T}{\partial t} = -\nabla \cdot (k\nabla T) + \nabla \cdot [Q_s + Q_e + Q_a] + Q_{diss} \quad (1)$$

where $T = T(x, y, z, t)$ is the temperature, ρ is the material density (in $kg \cdot m^{-3}$), C_p is the specific heat capacity (in $J \cdot kg^{-1} \cdot K^{-1}$), t is the time (in s), k is the thermal conductivity (in $Wm^{-1}K^{-1}$) and Q_{diss} is the power dissipated by CubeSat electronic equipment. To solve Eq. (1), diffuse radiation has been assumed, whilst a Dirichlet boundary condition ($T = T_0$) is assumed at $t_0 = 0$ s. A Neuman boundary condition to impose that the normal heat flux nulls is considered. The system is allowed to radiate heat into the surroundings. The external temperature is assumed equal to be equal to 4 K. The non-linearity is due to the time-varying nature of the thermal loads and to the fact that the thermal parameters of the materials can be temperature-dependent [7], [8]. Eq. (1) has been solved with Heat Transfer in Solids package from the finite element method (FEM) commercial software Comsol Multiphysics v5.5 (Comsol Inc., Burlinghton, MA, USA).

B. Mechanical Model

The equation that rule the mechanical deformations ($\boldsymbol{\epsilon}$ – strain vector) due to a given temperature gradient can be written as [7], [8]

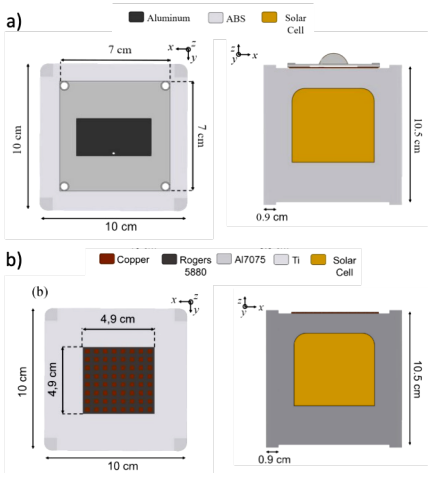

Fig. 4. a) Top and lateral views of the 3-D printed ABS curved patch antenna on the CubeSat z+-face. b) Top and lateral views of the CubeSat with the Ka-band array mounted on the z+-face.

$$\boldsymbol{\epsilon} = \frac{1+\nu}{E}\boldsymbol{\sigma} - \frac{\nu}{E}\boldsymbol{\sigma} + \alpha_{CTE}\nabla T \quad (2)$$

where ν is the Poisson's ratio, E is the Young's modulus (in Pa), whilst $\boldsymbol{\sigma}$ is the stress vector and α_{CTE} denotes the thermal expansion coefficient (CTE), whilst ∇T is the temperature gradient vector. In order to analyze the thermal strain vector of the two novel CubeSat antennas, the mechanical study has been carried out assuming linear thermoelasticity, isotropicity and following a damage-tolerant approach, as in [7], [8]. Furthermore, the von Mises stress (σ_{VM}), that are the second invariant of the stress tensor, are evaluated as figure of merit. Indeed, by analyzing σ_{VM}), it is possible to predict if the antenna system can be subject to any mechanical failure due to the induced thermal deformation [7], [8]. The thermal stress analysis has been performed in Comsol by relying on the Structural Mechanics module. The temperature field at a given time step, computed from the solution of Eq. (1) for the heat transfer problem, has been used to solve Eq. (2) in a one-way coupling scheme, as highlighted by Fig. 3.

IV. Results

The electromagnetic and radiation performances of the S-band and the Ka-band antennas have been studied. Then, the compliance and robustness of these communication tools has been studied from the thermal and mechanical point of view, considering how the space environment would affect the communication routines.

A. Antennas Characterization

The 3-D printed curved patch antenna for S-band CubeSat applications is characterized by a -10 dB bandwidth of about 14%, covering both the uplink and downlink bands, as it can be seen from Fig. 5a. The simulated data are compared with the experimental findings reported in [7]. The antenna has an average gain of about 6.7 dBi, as shown in Fig. 5b. The simulated radiation patterns are presented in Figs. 5c and 5d, compared to the experimental findings taken from [7]. The 3-D printed curved patch antenna for S-band CubeSat applications presents an efficiency of 96%. Furthermore, it must be reported that the design results in a size reduction along the resonant length of about 34% w.r.t. a common planar patch antenna. Not only, and most importantly, given the use of a non-conventional manufacturing techniques and the usage of the polymeric material, the final antenna design is characterized by a total weight of about 50 g. Given the

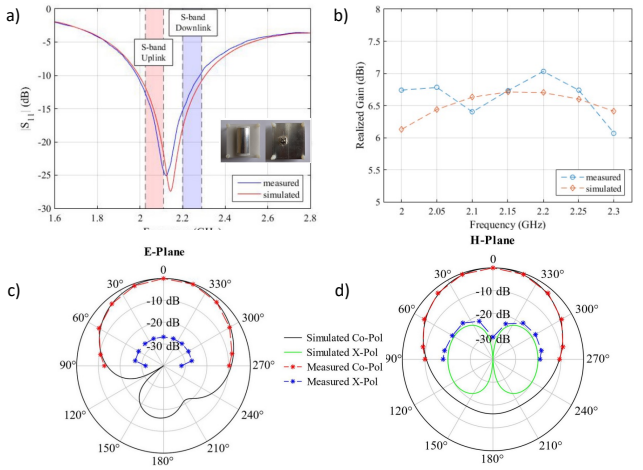

Fig. 5. a) Antenna S_{11}. b) Antenna gain in dBi. c) Antenna radiation pattern on the E-plane. d) Antenna radiation pattern on the H-plane.

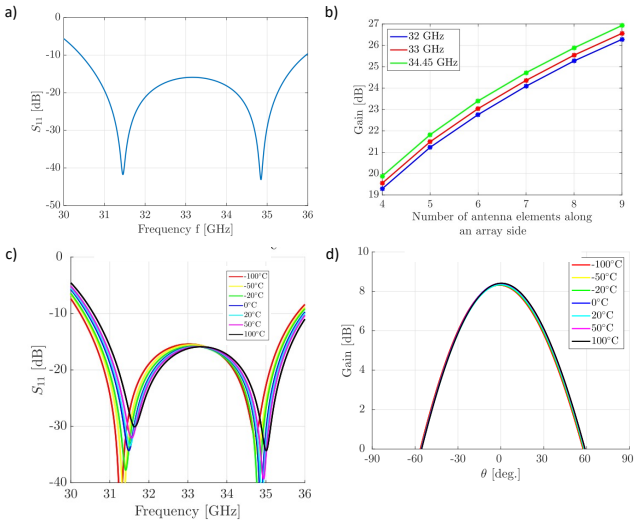

Fig. 6. a) Simulated S_{11}. b) Gain as a function of the number of antenna elements along an array side. c) S_{11} of the antenna element at different temperatures. d) Broadside gain over temperature.

satisfying performances and the lightweight, the presented antenna design results in a very appealing solution for CubeSat applications. Moreover, forecasting that plastic CubeSat may be used in future, the proposed 3-D printed curved patch antenna could be directly integrated in the chassis, thus easing the manufacturing process. Despite these pros, the antenna performances during a typical space mission must be verified.

As regards the Ka-band array for DSN CubeSat missions, a large 10 dB matching bandwdith of ~5.53 GHz (i.e., 16.6%) has been found, as shown in Fig. 6a. The antenna array is able to cover the whole Ka-band, thus being able to operate in both uplink and downlink conditions. A 4x4 antenna array is sufficient to reach a relatively high gain of 19-20 dBi for frequencies ranging from 32 to 34.45 GHz, as given in Fig. 6b.

B. Simulated Space Missions & Antennas Performances

The antennas performances variation during a typical CubeSat mission for both the wideband designs have been studied through a numerical multiphysics model.

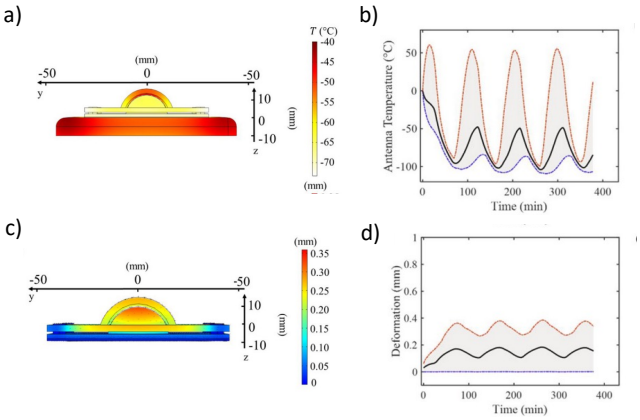

Fig. 7. a) Antenna temperature pattern (°C) during a cooling stage. b) Average antenna temperature, with overimposed deviation, versus the orbital cycles. c) Antenna displacement field (mm). d) Average displacement, with overimposed deviation, in the antenna versus the orbital cycles.

As regards the 3-D printed curved patch antenna, the pattern of the antenna surface temperature is shown in Fig. 7a. From the analysis of the average antenna temperature, it can be noticed that relevant temperature gradients (~6°C/cm) can establish between different part of the ABS antenna, as well as with the CubeSat chassis. By considering the average antenna temperature over time (Fig. 7b) it can be observed that during the orbits, the temperature ranges from more than 50°C to −100°C. The thermal states observed in Figs. 7a and 7b, result in induced thermal stresses. Relevant mechanical stresses are occurring in the bending region of both the top and bottom layer. On the other hand, during the orbital time, the Von Mises stresses result in a relatively narrow range of variation between $6-12$ MPa, reaching a maximum of ~ 100 MPa on the antenna edges in the top layer. As a result, the maximum antenna deformation is on the order of ~ 0.38 mm, occurring during the antenna cooling (Fig. 7c). The average displacement, on the other hand, ranges from 0.1 mm to 0.18 mm. Considering these numerical findings, by simulating the deformed antenna configuration, a difference of ~ 5 dB at the peak of the $|S_{11}|$ frequency response has been found. It must be reported that no detuning and bandwidth variation occurred. This is due to the relative narrow variation of the dielectric permittivity of the antenna substrate on the system temperature [7]. Therefore, the 3-D printed curved patch antenna performances are poorly affected by the thermo-mechanical deformation due to the harsh space environment.

For what concerns the Ka-band array for DSN CubeSat applications, it must be recalled that a linear variation of the permittivity pattern and of the copper electrical conductivity over temperature has been assumed. Considering the temperature pattern shown in Fig. 8a, it can be noticed that the range of variation is relatively narrow. Therefore, assuming an almost uniform temperature for the array, considering the average of the temperature with respect to the orbital time, Fig. 8b has been derived. Variation of the temperature of ± 20°C can be observed. Therefore, relying on these values, the impact of the array temperature on the S_{11} has been simulated and the findings are given in Fig. 6c. It can be noticed that as the temperature increases, the higher the S_{11}, whereas a left shift (~340 MHz) in frequency can be observed. Despite the frequency shift, the array still covers downlink ($31.8-32.3$ GHz) and uplink ($34.2-34.7$ GHz) frequency bands of the deep-space Ka band, with a value of the return

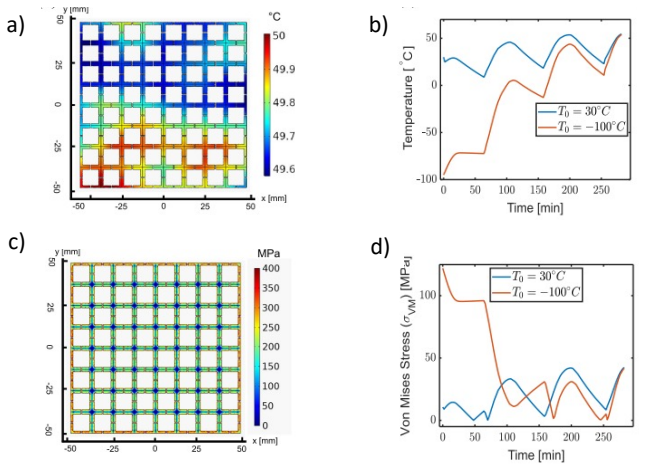

Fig. 8. a) 2D temperature distribution (in °C) on the xy-plane of the arrays. b) Average array temperature as a function of the orbital time. c) 2D pattern of the von Mises stresses on the xy-plane of the array. d) Average von Mises stresses as a function of the orbital time.

loss higher than 15 dB. For the temperature values that the antenna is supposed to face during a CubeSat mission (Fig. 8b), it must be reported that the gain is poorly affected (< 1 dB) by the different thermal conditions, as shown in Fig. 6d. These findings highlight that the proposed design as a good confidence level in terms of antenna performances for variable thermal conditions. Anyway, even though the thermal gradients in the system are relatively small (e.g., maximum 0.4 °C·cm^{-1} from Fig. 8a), induced thermal stresses and deformation can occur. For the Ka-band array a negligible bending of ~0.1-0.25 μm along the z-direction has been found. These deformations did not affect the radiating performances of the antenna array. However, the deformation is due to a pattern of stresses that are concentrated at the corners of the metal ring, and at the outer boundaries of the array. These von Mises stresses on the array elements are in the range of 47–120 Mpa. These values can result in a potential breaking and rupture condition of the bonding between the top and bottom layer of the array. However, with our simulations it has been possible to identify the ranges of mechanical stress, thus allowing to take countermeasures, such as the use of suitable glues approved for space applications [8].

V. Conclusion & Discussion

This work dealt with the presentation of different methodologies for designing innovative antennas for CubeSat applications. A 3D-printed curved stacked patch antenna working in the S-band has been designed, studied and characterized. Furthermore, a stacked patch antenna array working in the Ka-band has been designed and numerically studied. The variation of the antennas electromagnetic and radiation performances have been studied with a dedicated numerical multiphysics model that couples the thermal and mechanical conditions faced by the communication module during a simulated CubeSat mission. From our *in silico* studies, we found that the extreme temperature conditions and significant thermal gradients can induce relevant thermal stresses or deformation that can, in principle, ruin the antenna radiation performances. Therefore, it is mandatory to study the quality and feasibility of an antenna design (i.e., materials, geometry, etc.) considering all these aspects. It can be noticed that the temperature of a CubeSat system can be controlled, thus preventing any malfunctioning of the antenna element.

The proposed numerical multiphysics model could be used as an innovative quantitative framework for studying new design strategies for wideband, resilient, robust and effective CubeSat antennas.

References

[1] CubeSat Design Specification Rev. 13," California Polytechnic State University [Online]. Available: https://static1.squarespace.com/static/5418c831e4b0fa4ecac1bacd/t/56e9b62337013b6c063a655a/1458157095454/cds_rev13_final2.pdf, accessed on July 11, 2023..

[2] R. Baktur, "CubeSat Link Budget: Elements, calculations, and examples," *IEEE Antennas and Propagation Magazine*, vol. 64, no. 6, pp. 16-28, 2022.

[3] N. Chahat, et al., "Advanced cubesat antennas for deep space and earth science missions: A review," *IEEE Antennas and Propagation Magazine*, vol. 61, no. 5, pp. 37-46, 2019.

[4] M. El Hammoumi, et al., "A Wideband 5G CubeSat Patch Antenna," *IEEE Journal on Miniaturization for Air and Space Systems*, vol. 3, no. 2, pp. 47-52, 2022.

K. Trzebiatowski, et al., "Multibeam Antenna for Ka-Band CubeSat Connectivity Using 3-D Printed Lens and Antenna Array," *IEEE Antennas and Wireless Propagation Letters*, vol. 21, no. 11, pp. 2244-2248, 2022.

[5] D. Kim, et al., "Self-Deployable Circularly Polarized Phased Yagi–Uda Antenna Array Using 3-D Printing Technology for CubeSat Applications," *IEEE Antennas and Wireless Propagation Letters*. Vol. 21, no. 11, 2249-2253, 2022.

[6] G. Muntoni, et al., "A curved 3-D printed microstrip patch antenna layout for bandwidth enhancement and size reduction," *IEEE Antennas and Wireless Propagation Letters*, vol. 19, no. 7, pp. 1118-1122, 2020.

[7] G. Muntoni, et al., "A Curved 3D-Printed S-Band Patch Antenna for Plastic CubeSat," *IEEE Open Journal of Antennas and Propagation*, vol. 3, pp. 1351-1363, 2022.

[8] M. Simone, et al., "Optimized design and multiphysics analysis of a Ka-band stacked antenna for CubeSat applications," *IEEE Journal on Multiscale and Multiphysics Computational Techniques*, vol. 6, pp. 143-157, 2021.